Theory and experimental observation of hyperbolic media based on structural dispersions

Wenjie Ji,[1,2,*] Xiaoxi Zhou,[2,*] Hongchen Chu,[1] Jie Luo,[2,†] and Yun Lai[1,‡]

[1]*National Laboratory of Solid State Microstructures, School of Physics, and Collaborative Innovation Center of Advanced Microstructures, Nanjing University, Nanjing 210093, China*

[2]*School of Physical Science and Technology, Soochow University, Suzhou 215006, China*

(Received 17 February 2020; accepted 8 October 2020; published 26 October 2020)

Hyperbolic media usually possess large dissipation induced by the inherent imaginary part in the material dispersion of their metallic components. Here, we theoretically and experimentally demonstrate a route toward hyperbolic media with low dissipation: using structural dispersions. In a planar microwave waveguide filled with anisotropic dielectrics, we insert an array of metal wires and transform the original hybrid modes into pure transverse-electric modes. Interestingly, by engineering the structural dispersions such that waves are evanescent in one direction and propagating in the orthogonal direction, hyperbolic media with negligible loss can be achieved. Conical radiation pattern and negative refraction, which are characteristic phenomena of the hyperbolic media, have been numerically or experimentally demonstrated in microwaves. Our work opens an approach to utilize structural dispersions instead of material dispersions in realizing hyperbolic media with negligible loss.

DOI: 10.1103/PhysRevMaterials.4.105202

I. INTRODUCTION

Hyperbolic media [1–25] are a class of anisotropic materials, described by diagonal permittivity ε (or permeability μ) tensors with principal components having opposite signs. As a result, the equal frequency contour (EFC) in wave-vector space describes open hyperboloids. This leads to a salient feature of the hyperbolic media, that is, wave vectors span an unlimited range, that portends potential applications in the fields of high-resolution imaging [5–7], negative refraction [8,9], photonic density of states manipulation [10,11], thermal emission engineering [12], spontaneous emission enhancement [13,14], etc.

Traditionally, in optical and infrared regimes, the most common realization of hyperbolic media is metal (with negative-ε response)-dielectric composites [2,3], which generally suffer from large dissipative losses, thus limiting the performance of hyperbolic media. At terahertz and microwave frequencies, metals behave like perfect electric conductors (PECs), which do not support the negative-ε response. Therefore, artificial metallic structures have been proposed to attain effective negative-ε/μ response to construct the hyperbolic media at low frequencies [22–25], which however may exhibit undesired spatial dispersions and mode coupling effects [26]. Actually, almost all the above methods are based on material dispersions of metals at optical frequencies and spoof plasmonic structures at terahertz and microwave frequencies.

In this work, we theoretically and experimentally demonstrate a different route toward the hyperbolic media based on structural dispersions, which possesses the advantage of low dissipative loss. The structural dispersion, also known as the geometrical dispersion, is due to the role of geometry of the structures on wave propagation, such as the modal dispersion in bounded guided-wave structures [27]. Recent investigation of structural dispersions shows that effective electric response can be realized and engineered for transverse-electric (TE) modes in waveguides filled with isotropic dielectrics, based on which, low-loss effective ε-near-zero media and surface plasmon polaritons have been demonstrated [27–41]. However, most of the above investigation is focused on isotropic models supporting TE_n modes, and the principle is inapplicable in anisotropic models, because anisotropic dielectric-filled waveguides generally do not support TE_n modes [41–43]. Interestingly, here we find a route to transform hybrid waveguide modes to pure TE_n modes in an anisotropic waveguide by using metal wires. For verification, we construct a PEC parallel-plate waveguide (PPW), which is filled with alternately stacked two different dielectrics (serving as an effective anisotropic dielectric) and an array of metal wires (connecting the parallel PEC plates). It is found that within a certain frequency range, TE_n modes exhibiting different structural dispersions in different directions can be obtained. By engineering the structural dispersions, low-loss effective hyperbolic media are demonstrated with wave phenomena of negative refraction and conelike emission.

II. MODE TRANSFORMATION IN ANISOTROPIC WAVEGUIDES

Let us start with a PEC PPW filled with alternately stacked dielectric A (relative permittivity ε_A, width w_A) and dielectric B (relative permittivity ε_B, width w_B) with a lattice constant of $a = w_A + w_B$ along the x direction, as illustrated in Fig. 1. Here, we assume that a is much smaller than the wavelength in dielectrics A and B; thus, we can homogenize

*These authors contributed equally to this work.
†luojie@suda.edu.cn
‡laiyun@nju.edu.cn

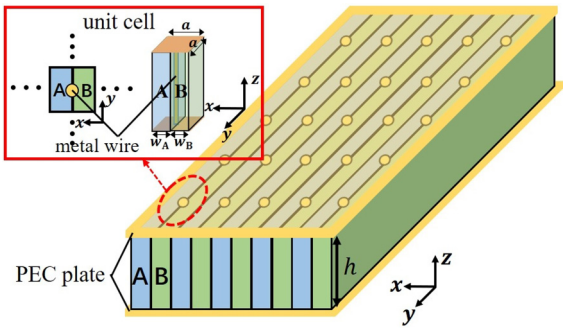

FIG. 1. Illustration of a dielectric stack-filled PPW model. The dielectric stack is composed of periodic dielectrics A and B layers along the x direction. An array of vertical metal wires is used to connect upper and lower PEC plates. The inset shows different perspectives of the PPW unit cell.

such a dielectric stack as an effective uniform anisotropic dielectric with $\varepsilon_x = \varepsilon_A\varepsilon_B a/(\varepsilon_B w_A + \varepsilon_A w_B)$ and $\varepsilon_y = \varepsilon_z = (\varepsilon_A w_A + \varepsilon_B w_B)/a$ [44,45]. At interfaces between dielectrics A and B, periodic thin metal wires are inserted, which connect the upper and low PEC plates, as illustrated in Fig. 1. Such an array of metal wires is used to transform waveguide modes, as we shall discuss as follows.

First, we analyze waveguide modes of the PPW in the absence of metal wires by calculating band structures based on the software COMSOL MULTIPHYSICS. Figure 2(a) presents the normalized eigenfrequency fa/c of the dielectrics tack-filled PPW (red dots) along the k_x and k_y directions, where c is speed of light in free space. The left inset shows the studied PPW unit cell, whose width is a in both the x and y directions. The height of the PPW is $h = 5a$ in the z direction. The relevant parameters of the dielectrics are chosen as $\varepsilon_A = 4$, $\varepsilon_B = 1$ and $w_A = w_B = 0.5a$, thus the corresponding effective anisotropic dielectric is characterized by $\varepsilon_x = 1.6$ and $\varepsilon_y = \varepsilon_z = 2.5$. In Fig. 2(a), band structures of the anisotropic dielectric-filled PPW are plotted as black lines, showing very good coincidence.

The lowest linear band in Fig. 2(a) corresponds to fundamental transverse electromagnetic (TEM) mode, whose electric field is polarized in the z direction. The propagation constant of such a TEM mode is independent of the PPW height h, indicating the absence of structural dispersions. Interestingly, structural dispersions occur in the modes of the second and third bands. For illustration, in Fig. 2(b), we present distributions of electric fields (arrows) and the z-component E_z (color) for the mode of $k_y = 0.15\,\pi/a$ and $fa/c = 0.0790$ in the second band (the left inset, on the y–z plane) and the mode of $k_x = 0.15\,\pi/a$ and $fa/c = 0.0921$ in the third band (the right inset, on the x–z plane). We find that electric fields are mainly polarized on the x–y plane, and the components E_x and E_y must vanish on the PPW PEC plates due to the continuity boundary condition. As a consequence, propagation constants of these modes rely on the height h, leading to structural dispersions.

However, within the frequency range of these modes, the PPW model cannot be homogenized as a structural dispersion-induced effective medium because of the following two reasons. First, there is more than one mode that can be excited,

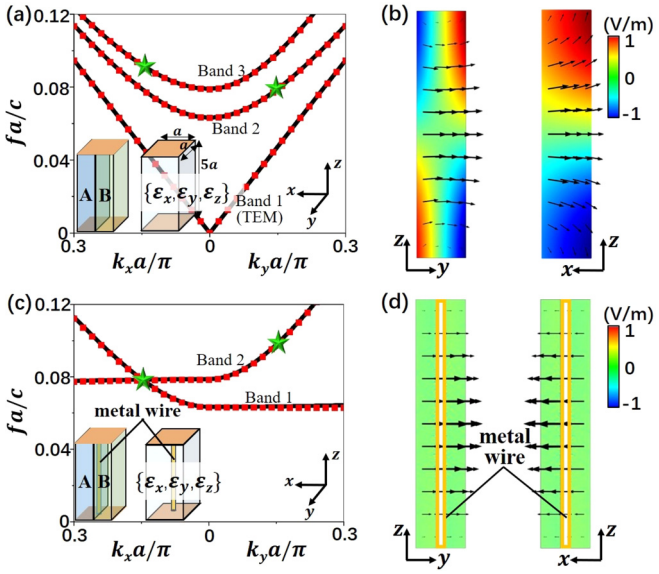

FIG. 2. (a), (c) Band structures of the dielectric stack-filled PPW (red dots) and the uniform anisotropic dielectric-filled PPW (black lines) (a) in the absence of metal wires, (c) in the existence of metal wires. The corresponding unit cells are illustrated by the insets. (b), (d) Snapshots of electric fields (arrows) and E_z of the waveguide modes. The left and right insets in (b) show the mode of $k_y = 0.15\,\pi/a$ and $fa/c = 0.0790$ in the second band and the mode of $k_x = 0.15\,\pi/a$ and $fa/c = 0.0921$ in the third band, respectively. The left and right insets in (d) show the mode of $k_x = 0.15\,\pi/a$ and $fa/c = 0.0788$ in the first band and the mode of $k_y = 0.15\,\pi/a$ and $fa/c = 0.0979$ in the second band, respectively. These modes are marked by green stars in (a) and (c).

because the fundamental TEM mode always exists. Thus, the single-mode condition [46–49], i.e., there is only one dominant mode in the PPW, is not satisfied. In this case, the PPW model cannot be homogenized as an effective medium with single-valued effective parameters, because different modes possess different structural dispersions. Second, during the homogenization, the $\mathrm{TE_n}$ mode (with electric fields polarized in the x–y plane) is required to be the dominant mode. Under this circumstance, there are only E_x, E_y, and H_z on the middle plane of the PPW, thus making it possible to regard this PPW model as a two-dimensional (2D) effective medium for transverse magnetic (TM) polarization (magnetic fields along the z direction) [26–37]. However, nonzero E_z is evidently seen in Fig. 2(b), indicating the hybrid modes instead of $\mathrm{TE_n}$ modes. Actually, such an anisotropic dielectric-filled PPW generally does not support $\mathrm{TE_n}$ modes [41–43]. As a consequence, the PPW model cannot be homogenized as an effective anisotropic medium.

Therefore, we need to transform these hybrid modes to $\mathrm{TE_n}$ modes, and simultaneously fulfill the single-mode condition. Inspired by previous works [26–38], we find that waveguide modes can be easily stirred by using metal wires to connect the upper and lower PEC plates. Such metal wires can short-circuit the E_z at relatively low frequencies. For demonstration, in Fig. 2(c) we recalculate the band structures by inserting a metal wire with radius of $0.1a$ in the center of each unit cell (see the insets). The red dots and black lines correspond

to the dielectric stack-filled PPW and the uniform anisotropic dielectric-filled PPW, respectively. Compared with the results in Fig. 2(a), the lowest linear band of the fundamental TEM mode disappears, and the bands of hybrid modes are changed dramatically. The dispersions along the k_x and k_y directions become strongly anisotropic.

Such strong anisotropic dispersion originates from waveguide mode transformation by metal wires. In the absence of metal wires, the waveguide modes possess the E_z component, leading to relatively weaker anisotropy, while when metal wires are placed inside the PPW, the upper and lower PEC plates connected by the metal wires would form a quasiequipotential system at low frequencies, therefore eliminating the E_z component. Pure $\mathrm{TE_n}$ modes with electric fields polarized on the $x-y$ plane can be obtained at relatively lower frequencies. The $\mathrm{TE_n}$ mode traveling along the x direction is dominated by ε_y, while the $\mathrm{TE_n}$ mode traveling along the y direction is dominated by ε_x. Since $\varepsilon_x \neq \varepsilon_y$, strong anisotropy of $\mathrm{TE_n}$ modes can be obtained near the cutoff frequencies, as seen in Fig. 2(c). It is worth noting that the metal wires are very thin, thus the $\mathrm{TE_n}$ modes will be almost unaffected by the metal wires because the electric fields are perpendicular to them [50].

For visualization of the transformed modes, we present the distributions of electric fields (arrows) and E_z (color) in Fig. 2(d). The left and right insets are related to the mode of $k_x = 0.15\,\pi/a$ and $fa/c = 0.0788$ in the first band and the mode of $k_y = 0.15\,\pi/a$ and $fa/c = 0.0979$ in the second band, respectively. It is seen that electric fields are polarized on the $x-y$ plane and the E_z is eliminated, indicating that the desired $\mathrm{TE_n}$ modes are obtained in the PPW. Actually, both the first and second bands correspond to the $\mathrm{TE_1}$ mode with E_x and E_y experiencing around π phase difference between the upper and lower PEC plates. Due to the in-plane anisotropy, the original $\mathrm{TE_1}$ mode in isotropic PPW splits into the two modes. We note that the flat band in the k_y (k_x) direction of the first (second) band corresponds to longitudinal modes that cannot be directly excited [51–53]. Consequently, for frequencies above the cutoff frequency of the $\mathrm{TE_1}$ mode (i.e., the bottom of the first band) and below the cutoff frequency of the $\mathrm{TE_2}$ mode (i.e., the bottom of the third band, not shown here), the single-mode condition is satisfied. In this case, such a PPW model can be regarded as a uniform effective anisotropic medium, whose structural dispersion-induced effective permittivity can be approximately calculated as [27]

$$\varepsilon_{x,\mathrm{eff}} = \varepsilon_A\varepsilon_B a/(\varepsilon_B w_A + \varepsilon_A w_B) - c^2/4f^2h^2 \quad \text{and}$$
$$\varepsilon_{y,\mathrm{eff}} = (\varepsilon_A w_A + \varepsilon_B w_B)/a - c^2/4f^2h^2. \tag{1}$$

According to Eq. (1), we can evaluate the cutoff frequency of the first band f_{c1} (or the second band f_{c2}) by imposing $\varepsilon_{y,\mathrm{eff}} = 0$ (or $\varepsilon_{x,\mathrm{eff}} = 0$), leading to $f_{c1}a/c \approx 0.0632$ (or $f_{c2}a/c \approx 0.0791$). The results coincide well with those obtained from the band structures in Fig. 2(c) (i.e., $f_{c1}a/c \approx 0.0631$ and $f_{c2}a/c \approx 0.0783$), thus confirming the validity of the homogenization of the PPW model and the validity of the effective parameters in Eq. (1).

It should be noted that we need to first homogenize the periodic dielectric stack, then calculate the effective parameters and cutoff frequencies based on structural dispersions. If this process is reversed, we will get wrong results. For example, if we first calculate the structural dispersion-induced effective parameters as $\varepsilon_{A(B),\mathrm{eff}} = \varepsilon_{A(B)} - c^2/4f^2h^2$, then substitute them into $\varepsilon_{x,\mathrm{eff}} = \varepsilon_{A,\mathrm{eff}}\varepsilon_{B,\mathrm{eff}} a/(\varepsilon_{B,\mathrm{eff}} w_A + \varepsilon_{A,\mathrm{eff}} w_B)$, we will have two cutoff frequencies regarding to $\varepsilon_{x,\mathrm{eff}} = 0$, that is, $f_{c2}a/c = 1/10\sqrt{\varepsilon_A} = 0.05$ and $1/10\sqrt{\varepsilon_B} = 0.1$. Evidently, the results do not agree with the simulation results in Fig. 2(c). Therefore, the formula of effective parameters in Eq. (1) is unique.

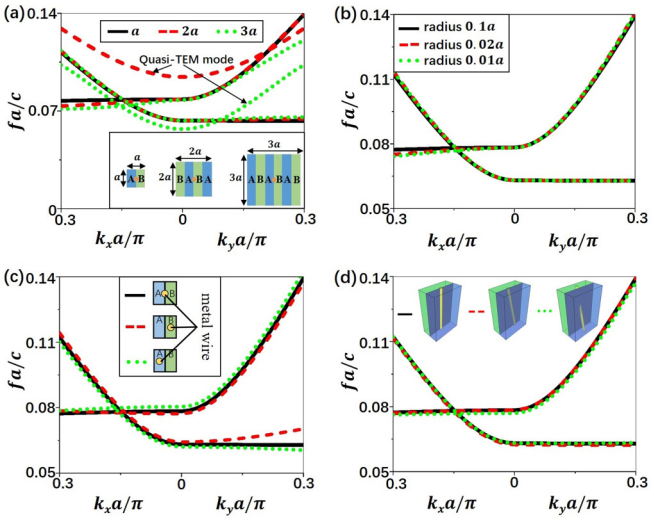

FIG. 3. Band structures of the dielectric stack-filled PPW model when (a) the lattice constant of the unit cell is changed as a (black), $2a$ (red), and $3a$ (green), (b) the radius of metal wires is chosen as $0.1a$ (black), $0.02a$ (red), and $0.01a$ (green), (c) the metal wire is located at center of the unit cell (black), the dielectric A (red), and the dielectric B (green), and (d) the orientation of metal wires is changed. The corresponding unit cells are illustrated in the insets.

It is also worth noting that the functionality of metal wires here is different from that in previous works of isotropic models [26–37]. In an isotropic dielectric-filled PPW, $\mathrm{TE_n}$ modes are naturally supported even without metal wires. Metal wires are required only at interfaces between different filling materials to short-circuit the E_z, so as to prevent the coupling from the dominant $\mathrm{TE_n}$ modes to other undesired modes. However, in the anisotropic dielectric-filled PPW, generally there are no $\mathrm{TE_n}$ modes in the absence of metal wires [41–43]. Therefore, the metal wires are essential for the realization of $\mathrm{TE_n}$ modes in anisotropic models.

Actually, in order to guarantee good performances, a certain density of metal wires is required. If the density is too low, hybrid modes and the quasi-TEM mode will reappear. To show the effects of the density, band structures of the dielectric stack-filled PPWs with larger unit cells are calculated in Fig. 3(a). Since there is only one metal wire in the center of each unit cell, enlarging the unit cell implies the decrease of the metal wire density. The black, red, and green lines in Fig. 3(a) denote band structures for the cases with lattice constants of a, $2a$, and $3a$, respectively. Here, a is the lattice constant of the unit cell in Fig. 2. The radius of metal wires in all the three cases is $0.1a$, the same as that in Fig. 2. It is seen from Fig. 3(a) that with the decrease of the metal wire density, hybrid modes and the quasi-TEM mode will gradually

reemerge, which tend to be the same as those in Fig. 2(a) when the density is further decreased.

Moreover, we also study the influences of the radius, position, and orientation of the metal wires. In Fig. 3(b), band structures of the dielectric stack-filled PPW are recalculated by choosing the radius of metal wires as $0.1a$ (black lines), $0.02a$ (red lines), and $0.01a$ (green lines), showing almost unchanged band structures. Figure 3(c) displays the band structures when metal wires are placed in the center of the unit cell (i.e., at the interface between dielectrics A and B, black lines), the dielectric B (red lines) and the dielectric A (green lines), also showing very weak influence. In addition, in Fig. 3(d), the orientation of metal wires is changed (see the insets), still showing almost unchanged band structures. Apparently, the above results reveal that the waveguide modes are mainly affected by the density of metal wires, and have very weak dependence on the radius, position, and orientation of metal wires.

Besides the comprehensive picture based on the above band diagram, we can also understand the proposed hyperbolic media in an alternative way. It is known that a PPW filled with an isotropic dielectric supports TE_n modes, whose cutoff frequency relies on the permittivity of the filling dielectric. Here, through adjusting the permittivity, we have constructed two kinds of isotropic dielectric-loaded PPWs with different cutoff frequencies of TE_n modes. One is below and the other is above the working frequency, indicating the PPW working as a medium with positive and negative permittivity, respectively. Then, through periodically stacking the two kinds of effective media in the deep-subwavelength scale as the conventional metal-dielectric multilayered hyperbolic media, we will get a model of PPW filled with a dielectric multilayer stack consisting of two different dielectrics (as the model shown in Fig. 1). However, the multilayer stack would change the waveguide modes, leading to hybrid modes with E_z component. Therefore, metal wires are needed to eliminate the E_z component and transform the hybrid modes to TE_n modes. Finally, we will obtain effective hyperbolic metamaterial in the waveguide model, similar to the conventional metal-dielectric multilayered hyperbolic media.

III. WAVE PHENOMENA BASED ON EFFECTIVE HYPERBOLIC MEDIA

Following the discussion in the previous section, we aim at realizing 2D effective hyperbolic media based on the structural dispersions. Due to the in-plane anisotropy of the dielectric stack-filled PPW model, TE_n modes exhibit different structural dispersions in different directions, thus leading to anisotropic propagation behaviors of electromagnetic waves in the waveguide. Moreover, for the TE_1 mode, only E_x, E_y, and H_z exist on the middle plane of the PPW. In this situation, we can homogenize the PPW model as a 2D effective medium for TM polarization (magnetic fields along the z direction), whose effective parameters are characterized by Eq. (1). Interestingly, the dispersions in Fig. 2(c) indicate that for the working frequency between cutoff frequencies of the first two bands (i.e., $f_{c1} < f < f_{c2}$), the TE_1 mode propagating along the y (or x) direction will be evanescent (or propagating). In this way, we can obtain the effective hyperbolic media.

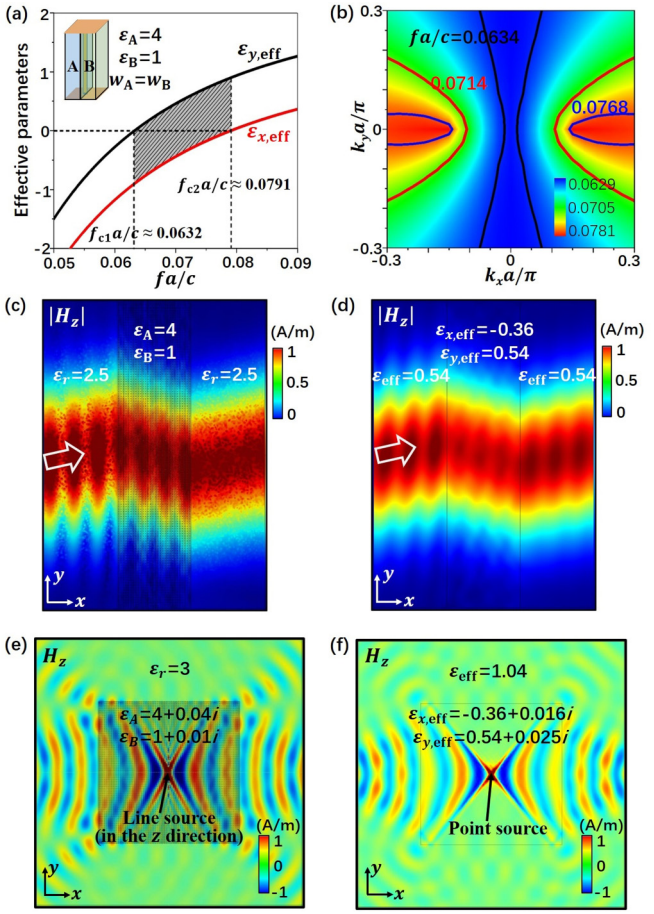

FIG. 4. (a) Effective parameters of the dielectric stack-filled PPW model, whose unit cell is illustrated by the inset. (b) EFCs of the PPW model. The black, red, and blue lines correspond to the frequencies $fa/c = 0.0634$, 0.0714, and 0.0768, respectively. (c) Distributions of magnetic-field amplitudes $|H_z|$ on the middle plane of the PPW under the illumination of a Gaussian beam of the TE_1 mode. (d) Distributions of $|H_z|$ in the effective 2D model under the illumination of a TM-polarized Gaussian beam. The incident angle in (c) and (d) is 12°. (e) Distributions of magnetic fields H_z on the middle plane of the PPW when a magnetic-current line source is placed in the center along the z direction. (f) Distributions of H_z in the effective 2D model when a magnetic-monopole point source is placed in the center. The working frequency in (c)–(f) is $fa/c = 0.0714$.

In Fig. 4(a), effective parameters of the dielectric stack-filled PPW model are plotted according to Eq. (1). The unit cell is illustrated by the inset, which is the same as that in Fig. 2(c). It is seen from Fig. 4(a) that in the frequency range of $f_{c1} < f < f_{c2}$ (the shaded area), we have $\varepsilon_{x,\mathrm{eff}} < 0$ and $\varepsilon_{y,\mathrm{eff}} > 0$, indicating broadband hyperbolic media. Figure 4(b) shows the EFCs of the PPW model at frequencies $fa/c = 0.0634$ (black lines), 0.0714 (red lines), and 0.0768 (blue lines), confirming the hyperbolic dispersions.

Here, we take two examples to show wave phenomena of the structural dispersion-induced hyperbolic media. The first example in Fig. 4(c) shows negative refraction in the PPW model. A Gaussian beam of the TE_1 mode is incident from the PPW filled with an isotropic dielectric (relative permittivity

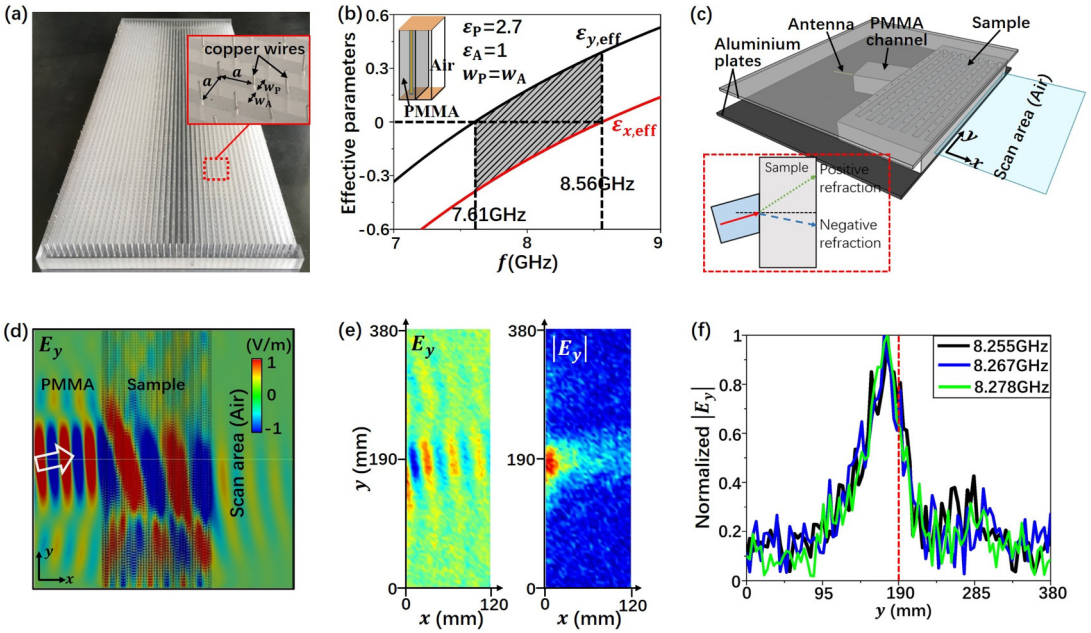

FIG. 5. (a) Photograph of the fabricated dielectric-stack sample, consisting of periodic PMMA and air with width $w_P = w_A = 2\,mm$ and height $h = 14.5\,mm$. Periodic tin-plated copper wires (radius 0.15 mm) are vertically inserted in the PMMA with a separation distance of 4 mm. (b) Effective parameters of the PMMA-air stack-filled PPW model, whose unit cell is illustrated by the inset. (c) Schematic of the experimental setup. The fabricated PMMA-air stack is placed between two parallel aluminum plates. The inset illustrates the positive refraction and negative refraction. (d) Simulated E_y distribution on the middle plane of the PPW model illuminated with a Gaussian beam of the TE_1 mode under an incident angle of 8.5°. (e) Measured distributions of E_y (left) and $|E_y|$ (right) in the scan area at 8.255 GHz. (f) Normalized $|E_y|$ distribution on the exiting surface of PMMA-air stack at frequencies 8.255 GHz (black lines), 8.267 GHz (blue lines), and 8.278 GHz (green lines).

$\varepsilon_r = 2.5$) under an incident angle of 12° at $fa/c = 0.0714$. From the distributions of magnetic-field amplitudes $|H_z|$ on the middle plane of the PPW in Fig. 4(c), clear negative refraction is observed. For comparison, we also simulate the 2D effective medium model in Fig. 4(d) by illuminating the central effective hyperbolic medium ($\varepsilon_{x,\text{eff}} = -0.36$ and $\varepsilon_{y,\text{eff}} = 0.54$) with a TM-polarized Gaussian beam, also showing evident negative refraction behavior. In the second example, we place a magnetic-current line source in the center of the dielectric stack-filled PPW, as presented in Fig. 4(e). The H_z distribution on the middle plane of the PPW shows a highly anisotropic conelike emission pattern at $fa/c = 0.0714$. Waves are propagating within this cone and are evanescent outside this cone. Such a conelike emission pattern is also observed in the 2D effective hyperbolic medium ($\varepsilon_{x,\text{eff}} = -0.36 + 0.016i$ and $\varepsilon_{y,\text{eff}} = 0.54 + 0.025i$) under the illumination of a magnetic-monopole point source in the center, as shown in Fig. 4(f). Here, a small amount of material loss is introduced to avoid infinitely large wave vectors and infinite density modes [21].

Next, we use the first example, i.e., the negative refraction, to demonstrate the effectiveness of our approach in microwave experiments. We fabricated a dielectric stack consisting of periodic polymethyl methacrylate (PMMA, $\varepsilon_P = 2.7$, $w_P = 2$ mm) and air ($\varepsilon_A = 1$, $w_A = 2$ mm), as shown by the photograph in Fig. 5(a). The size of the sample is 160 mm × 400 mm × 14.5 mm (height). Periodic tin-plated copper wires (radius 0.15 mm) are vertically inserted in the PMMA with a lattice constant of 4 mm. Figure 5(b) presents the effective parameters of the PMMA air stack-filled PPW model based on Eq. (1), showing a hyperbolic region from 7.61 to 8.56 GHz. Figure 5(c) shows the schematic of the experimental setup. The fabricated PMMA-air stack is placed between two parallel aluminum plates of a PPW. On the left surface, a PMMA channel with a tilt angle of 8.5° is used to guide the incident beam, because the working frequency is below the cutoff frequency of the TE_1 mode in empty PPW. A horizontally oriented antenna connected to PNA Network Analyzer N5224B is placed nearby the end surface of the PMMA channel to excite the TE_1 mode (see details in Ref. [54]). Here, the center of the exiting surface of the PMMA channel is aligned to the centerline of the PMMA-air stack, so that we can easily tell the refraction behavior by measuring the fields on the existing surface of the PMMA-air stack (i.e., the right surface). Positive refraction happens if the fields on the existing surface are mainly concentrated above the centerline, otherwise, negative refraction occurs, as illustrated by the inset in Fig. 5(c).

Figure 5(d) displays the simulated E_y distribution on the middle plane of the PPW, showing the negative refraction on the surfaces of the PMMA-air stack. Here, the electric fields in the scan region (i.e., air) decay quickly because there is no confinement by aluminum plates, and beam spreads into the other directions. Figure 5(e) show the measured distributions of E_y (left) and $|E_y|$ (right) in the scan area at 8.255 GHz. We observe that the electric fields are mainly concentrated below the centerline ($y = 190\,mm$) of the PMMA-air stack. Furthermore, the normalized $|E_y|$ along the existing surface of the PMMA-air stack at 8.255 GHz (black lines), 8.267 GHz (blue lines), and 8.278 GHz (green lines) is plotted in Fig. 5(f). Apparently, all positions of the maximal $|E_y|$ for the three

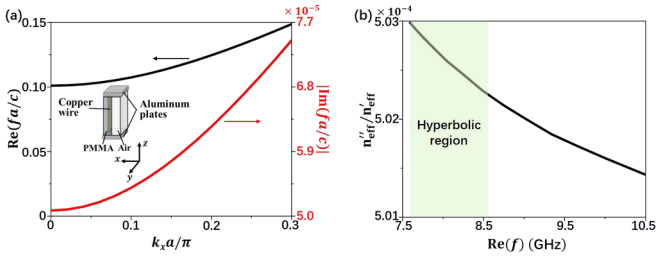

FIG. 6. (a) Real and imaginary parts of the normalized eigenfrequency along the k_x direction in the existence of material losses. (b) Ratio of the imaginary part n''_{eff} to the real part n'_{eff} of the effective refractive index for modes along the k_x direction. The green area denotes the hyperbolic region.

frequencies are below the centerline, demonstrating the negative refraction.

Finally, we take material losses into consideration. In calculations, electrical conductivities of copper wires and aluminum plates are set as $\sigma_{\text{Cu}} = 5.9 \times 10^7$ S/m and $\sigma_{\text{Al}} = 3.8 \times 10^7$ S/m, respectively. Relative permittivities of PMMA and air are assumed to be $\varepsilon_{\text{P}} = 2.7 + 0.0027i$ and $\varepsilon_{\text{A}} = 1 + 0.001i$, respectively. Figure 6(a) presents the complex eigenfrequency along the k_x direction, showing that the imaginary part is much smaller than the real part. Considering that the working frequency is relatively low, the effective refractive index for modes along the k_x direction can be approximately evaluated as $n_{\text{eff}} = ck_x/2\pi f$ [47,55]. In Fig. 6(b), the ratio of the imaginary part n''_{eff} to the real part n'_{eff} of the effective refractive index is plotted, which indicates that the imaginary part is four orders of magnitude smaller than the real part in the hyperbolic region (green area). These results clearly confirm the low-loss property of the proposed hyperbolic media.

For practical applications, there are several ways to increase the operating frequency range. For example, through the increasing of the permittivity contrast of dielectrics inside the PPW (i.e., increasing the effective anisotropy of the dielectric stack), the operating frequency range can be significantly improved. If we use alumina (relative permittivity ∼9) to replace the PMMA in experiments, the operating frequency range will be tripled. In addition, through the engineering of the filling ratio of dielectric components, as well as the height of the PPW, the working frequency range can be further increased.

IV. CONCLUSIONS

In conclusion, we have proposed an approach to design low-loss hyperbolic media based on structural dispersions instead of material dispersions in traditional approaches. It is found that the waveguide modes in dielectric stack-filled PPWs can be transformed from hybrid modes to TE_{n} modes with strongly anisotropic structural dispersions by exploiting an array of metal wires. By engineering the structure dispersions, the TE_{n} modes are evanescent in one direction and propagating in another direction, thus effective hyperbolic media are obtained. Furthermore, negative refraction in the structural dispersion-induced hyperbolic media is demonstrated in both simulations and experiments. Although our experimental demonstration is performed at microwave frequencies, the principle can be generalized to higher frequencies. Our work provides a convenient approach for low-loss highly anisotropic media, paving the road to advanced manipulation of electromagnetic waves.

ACKNOWLEDGMENTS

National Key R&D Program of China (Grant No. 2017YFA0303702), National Natural Science Foundation of China (Grants No. 11704271, No. 61671314, and No. 11974176), Natural Science Foundation of Jiangsu Province (Grant No. BK20170326), Natural Science Foundation for Colleges and Universities in Jiangsu Province of China (Grant No. 17KJB140019), the Priority Academic Program Development (PAPD) of Jiangsu Higher Education Institutions.

[1] D. Smith and D. Schurig, Electromagnetic Wave Propagation in Media with Indefinite Permittivity and Permeability Tensors, Phys. Rev. Lett. **90**, 077405 (2003).
[2] A. Poddubny, I. Iorsh, P. Belov, and Y. Kivshar, Hyperbolic metamaterials, Nat. Photonics **7**, 948 (2013).
[3] O. Takayama and A. V. Lavrinenko, Optics with hyperbolic materials, J. Opt. Soc. Am. B **36**, F38 (2019).
[4] J. Sun, N. M. Litchinitser, and J. Zhou, Indefinite by nature: From ultraviolet to terahertz, ACS Photonics **1**, 293 (2014).
[5] D. Lu and Z. Liu, Hyperlenses and metalenses for far-field super-resolution imaging, Nat. Commun. **3**, 1205 (2012).
[6] I. I. Smolyaninov, Y. J. Hung, and C. C. Davis, Magnifying superlens in the visible frequency range, Science **315**, 1699 (2007).
[7] Z. Liu, H. Lee, Y. Xiong, C. Sun, and X. Zhang, Far-field optical hyperlens magnifying sub-diffraction-limited objects, Science **315**, 1686 (2007).
[8] J. Yao, Z. Liu, Y. Liu, Y. Wang, C. Sun, G. Bartal, A. M. Stacy, and X. Zhang, Optical negative refraction in bulk metamaterials of nanowires, Science **321**, 930 (2008).
[9] A. A. High, R. C. Devlin, A. Dibos, M. Polking, D. S. Wild, J. Perczel, N. P. de Leon, M. D. Lukin, and H. Park, Visible-frequency hyperbolic metasurface, Nature (London) **522**, 192 (2015).
[10] O. D. Miller, S. G. Johnson, and A. W. Rodriguez, Effectiveness of Thin Films in Lieu of Hyperbolic Metamaterials in the Near Field, Phys. Rev. Lett. **112**, 157402 (2014).
[11] I. V. Iorsh, A. N. Poddubny, P. Ginzburg, P. A. Belov, and Y. S. Kivshar, Compton-Like Polariton Scattering in Hyperbolic Metamaterials, Phys. Rev. Lett. **114**, 185501 (2015).
[12] S. A. Biehs, M. Tschikin, and P. Ben-Abdallah, Hyperbolic Metamaterials as an Analog of a Blackbody in the Near Field, Phys. Rev. Lett. **109**, 104301 (2012).

[13] M. A. Noginov, H. Li, Y. A. Barnakov, D. Dryden, G. Nataraj, G. Zhu, C. E. Bonner, M. Mayy, Z. Jacob, and E. E. Narimanov, Controlling spontaneous emission with metamaterials, Opt. Lett. **35**, 1863 (2010).

[14] H. N. Krishnamoorthy, Z. Jacob, E. Narimanov, I. Kretzschmar, and V. M. Menon, Topological transitions in metamaterials, Science **336**, 205 (2012).

[15] J. Luo, Y. Xu, H. Chen, B. Hou, W. Lu, and Y. Lai, Oblique total transmissions through epsilon-near-zero metamaterials with hyperbolic dispersions, EPL (Europhys. Lett.) **101**, 44001 (2013).

[16] P. Li, I. Dolado, F. J. Alfaro-Mozaz, F. Casanova, L. E. Hueso, S. Liu, J. H. Edgar, A. Y. Nikitin, S. Vélez, and R. Hillenbrand, Infrared hyperbolic metasurface based on nanostructured van der Waals materials, Science **359**, 892 (2018).

[17] W. Ma, P. Alonso-González, S. Li, A. Y. Nikitin, J. Yuan, J. Martín-Sánchez, J. Taboada-Gutiérrez, I. Amenabar, P. Li, S. Vélez, C. Tollan, Z. Dai, Y. Zhang, S. Sriram, K. Kalantar-Zadeh, S. Lee, R. Hillenbrand, and Q. Bao, In-plane anisotropic and ultra-low-loss polaritons in a natural van der Waals crystal, Nature (London) **562**, 557 (2018).

[18] J. S. Smalley, F. Vallini, S. A. Montoya, L. Ferrari, S. Shahin, C. T. Riley, B. Kanté, E. E. Fullerton, Z. Liu, and Y. Fainman, Luminescent hyperbolic metasurfaces, Nat. Commun. **8**, 13793 (2017).

[19] Y. Yang, L. Jing, L. Shen, Z. Wang, B. Zheng, H. Wang, E. Li, N. Shen, T. Koschny, C. M. Soukoulis, and H. Chen, Hyperbolic spoof plasmonic metasurfaces, NPG Asia Mater. **9**, e428 (2017).

[20] S. S. Kruk, Z. J. Wong, E. Pshenay-Severin, K. O'Brien, D. N. Neshev, Y. S. Kivshar, and X. Zhang, Magnetic hyperbolic optical metamaterials, Nat. Commun. **7**, 11329 (2016).

[21] A. S. Potemkin, A. N. Poddubny, P. A. Belov, and Y. S. Kivshar, Green function for hyperbolic media, Phys. Rev. A **86**, 023848 (2012).

[22] D. R. Smith, D. Schurig, J. J. Mock, P. Kolinko, and P. Rye, Partial focusing of radiation by a slab of indefinite media, Appl. Phys. Lett. **84**, 2244 (2004).

[23] J. Sun, L. Kang, R. Wang, L. Liu, L. Sun, and J. Zhou, Low loss negative refraction metamaterial using a close arrangement of split-ring resonator arrays, New J. Phys. **12**, 083020 (2010).

[24] A. V. Shchelokova, D. S. Filonov, P. V. Kapitanova, and P. A. Belov, Magnetic topological transition in transmission line metamaterials, Phys. Rev. B **90**, 115155 (2014).

[25] X. Yin, H. Zhu, H. Guo, M. Deng, T. Xu, Z. Gong, X. Li, Z. H. Hang, C. Wu, H. Li, S. Chen, L. Zhou, and L. Chen, Hyperbolic metamaterial devices for wavefront manipulation, Laser Photonics Rev. **13**, 1800081 (2019).

[26] S. I. Maslovski and M. G. Silveirinha, Nonlocal permittivity from a quasistatic model for a class of wire media, Phys. Rev. B **80**, 245101 (2009).

[27] C. Della Giovampaola and N. Engheta, Plasmonics without negative dielectrics, Phys. Rev. B **93**, 195152 (2016).

[28] C. Sheng, H. Liu, Y. Wang, S. N. Zhu, and D. A. Genov, Trapping light by mimicking gravitational lensing, Nat. Photonics **7**, 902 (2013).

[29] B. Edwards, A. Alù, M. Young, M. Silveirinha, and N. Engheta, Experimental Verification of Epsilon-Near-Zero Metamaterial Coupling and Energy Squeezing Using a Microwave Waveguide, Phys. Rev. Lett. **100**, 033903 (2008).

[30] E. J. R. Vesseur, T. Coenen, H. Caglayan, N. Engheta, and A. Polman, Experimental Verification of n = 0 Structures for Visible Light, Phys. Rev. Lett. **110**, 013902 (2013).

[31] M. Zhou, L. Shi, J. Zi, and Z. Yu, Extraordinarily Large Optical Cross Section for Localized Single Nanoresonator, Phys. Rev. Lett. **115**, 023903 (2015).

[32] R. Liu, C. M. Roberts, Y. Zhong, V. A. Podolskiy, and D. Wasserman, Epsilon-near-zero photonics wires, ACS Photonics **3**, 1045 (2016).

[33] Z. Li, L. Liu, H. Sun, Y. Sun, C. Gu, X. Chen, Y. Liu, and Y. Luo, Effective Surface Plasmon Polaritons Induced by Modal Dispersion In A Waveguide, Phys. Rev. Appl. **7**, 044028 (2017).

[34] I. Liberal, A. M. Mahmoud, Y. Li, B. Edwards, and N. Engheta, Photonic doping of epsilon-near-zero media, Science **355**, 1058 (2017).

[35] F. R. Prudêncio, J. R. Costa, C. A. Fernandes, N. Engheta, and M. G. Silveirinha, Experimental verification of 'waveguide' plasmonics, New J. Phys. **19**, 123017 (2017).

[36] Z. Li, Y. Sun, K. Wang, J. Song, J. Shi, C. Gu, L. Liu, and Y. Luo, Tuning the dispersion of effective surface plasmon polaritons with stacklayer systems, Opt. Express **26**, 4686 (2018).

[37] Y. Li and Z. Zhang, Experimental Verification of Guided-Wave Lumped Circuits Using Waveguide Metamaterials, Phys. Rev. Appl. **9**, 044024 (2018).

[38] Y. Zhang, Y. Luo, J. B. Pendry, and B. Zhang, Transformation-Invariant Metamaterials, Phys. Rev. Lett. **123**, 067701 (2019).

[39] Y. Li, I. Liberal, and N. Engheta, Structural dispersion–based reduction of loss in epsilon-near-zero and surface plasmon polariton waves, Sci. Adv. **5**, eaav3764 (2019).

[40] C. Wang, H. Wang, L. Shen, R. Abdi-Ghaleh, M. Y. Musa, Z. Xu, and B. Zheng, Structure-induced hyperbolic dispersion in waveguides, IEEE Trans. Antennas Propag. **67**, 5463 (2019).

[41] W. Ji, J. Luo, and Y. Lai, Extremely anisotropic epsilon-near-zero media in waveguide metamaterials, Opt. Express **27**, 19463 (2019).

[42] F. E. Gardiol, Anisotropic slabs in rectangular waveguides, IEEE Trans. Microw. Theory **18**, 461 (1970).

[43] V. A. Podolskiy and E. E. Narimanov, Strongly anisotropic waveguide as a nonmagnetic left-handed system, Phys. Rev. B **71**, 201101(R) (2005).

[44] V. A. Markel, Introduction to the Maxwell Garnett approximation: tutorial, J Opt. Soc. A **33**, 1244 (2016).

[45] J. Luo, P. Xu, and L. Gao, Directive emission based on one-dimensional metal heterostructures, J. Opt. Soc. Am. B **29**, 35 (2012).

[46] W. Śmigaj and B. Gralak, Validity of the effective-medium approximation of photonic crystals, Phys. Rev. B **77**, 235445 (2008).

[47] J. Luo, Y. Yang, Z. Yao, W. Lu, B. Hou, Z. H. Hang, C. T. Chan, and Y. Lai, Ultratransparent Media and Transformation Optics with Shifted Spatial Dispersions, Phys. Rev. Lett. **117**, 223901 (2016).

[48] J. Luo and Y. Lai, Near-perfect absorption by photonic crystals with a broadband and omnidirectional impedance-matching property, Opt. Express **27**, 15800 (2019).

[49] S. Li, Y. Wang, W. Zhang, W. Lu, B. Hou, J. Luo, and Y. Lai, Observation of wide-angle impedance matching in terahertz photonic crystals, New J. Phys. **22**, 023033 (2020).

[50] J. B. Pendry, A. J. Holden, D. J. Robbins, and W. J. Stewart, Low frequency plasmons in thin-wire structures, J. Phys.: Condens. Matter **10**, 4785 (1998).

[51] X. Huang, Y. Lai, Z. H. Hang, H. Zheng, and C. T. Chan, Dirac cones induced by accidental degeneracy in photonic crystals and zero-refractive-index materials, Nat. Mater. **10**, 582 (2011).

[52] X. Zhang and Y. Wu, Effective medium theory for anisotropic metamaterials, Sci. Rep. **5**, 7892 (2015).

[53] Y. Yang, Z. Jia, T. Xu, J. Luo, Y. Lai, and Z. H. Hang, Beam splitting and unidirectional cloaking using anisotropic zero-index photonic crystals, Appl. Phys. Lett. **114**, 161905 (2019).

[54] See Supplemental Material at http://link.aps.org/supplemental/10.1103/PhysRevMaterials.4.105202 for band structures of the PPW in the absence of metal wires, details of the antenna and PMMA channel in experiments, negative refraction under large incident angles, positive refraction at frequencies outside the hyperbolic region.

[55] F. J. Lawrence, C. M. de Sterke, L. C. Botten, R. C. McPhedran, and K. B. Dossou, Modeling photonic crystal interfaces and stacks: impedance-based approaches, Adv. Opt. Photonics **5**, 385 (2013).